

Infrared surface plasmon resonance in a subwavelength metallic grating under illumination at a large incidence angle

Sookyong Roh,¹ Hwi Kim,^{2,*} and ByoungHo Lee¹

¹National Creative Research Center for Active Plasmonics Application Systems, Inter-University Semiconductor Research Center and School of Electrical Engineering, Seoul National University, Gwanak-Gu Gwanakro 599, Seoul, 151-744, South Korea

²Department of Electronics and Information Engineering, College of Science and Technology, Sejong Campus, Korea University, Jochiwon-eup, Yeongi-gun, Chungcheongnam-do 339-700, South Korea

*Corresponding author: hwikim@korea.ac.kr

Received February 7, 2011; revised April 16, 2011; accepted May 16, 2011;
posted May 17, 2011 (Doc. ID 142308); published June 10, 2011

Under the condition of illumination at a large incidence angle, surface plasmon (SP) resonances in the conventional Kretschmann configuration occur in the visible wavelength region. In this paper, we show that a subwavelength metallic binary grating that was specifically designed can induce IR SP resonance (SPR) effectively under the same illumination condition. We analyze the structural controllability of IR SPR by subwavelength metallic binary gratings and propose an optimal design of subwavelength grating structures for IR SPR under illumination at a large incidence angle. A numerical design method combining the rigorous coupled-wave analysis and the genetic algorithm is devised. © 2011 Optical Society of America

OCIS codes: 240.6680, 280.4788, 060.2370.

1. INTRODUCTION

Surface plasmons (SPs) are electromagnetic surface modes resonantly induced on metal–dielectric interfaces strongly coupled to surface charge oscillations. As SP resonance (SPR) is highly sensitive to environmental refractive index variations, it is used for various sensing applications [1–3]. Typically, SPR on a flat metal–dielectric interface occurs in visible or near-IR wavelength bands. Therefore, numerous SPR sensors have been developed for sensing with visible light [1,4]. However, using IR SPR for sensing applications could provide advantageous features in sensitivity enhancement and integration with well-established IR fiber optics technology. Longer-wavelength SPR is more sensitive to environmental refractive index variations than short-wavelength SPR because the SP waves penetrate more deeply into the sensing medium. For fiber optic SPR sensors [4,5], various approaches using diffraction gratings [5,6] or high-refractive-index substrates [7] have been developed to obtain IR SPR. Although we can obtain IR SPR using diffraction gratings, its sensitivity to environmental refractive index variations tends to degrade [6,8]. For example, the Bragg grating embedded in the core of fiber optic SPR sensors can be designed to couple the guided optical modes to the hybrid SP mode at IR wavelengths. However, the sensitivity of the hybrid SP mode is inferior to that of pure SP modes [9]. By using a high-refractive-index dielectric substrate in an SPR sensor, we can induce SPR in near-IR wavelengths, but the measurable range of the environmental refractive index would shift to values higher than those of general aqueous sensing mediums [7].

Fundamental structures sustaining IR SPR for high-performance sensing applications are rarely reported, and there is a strong need for the topic to be investigated. In this

paper, we propose an IR SPR structure with high sensitivity for aqueous sensing medium and analyze the structural controllability of IR SPR obtained by the proposed structure under large angle illumination. The condition of large angle illumination is important from a practical point of view because most fiber optic or waveguide-based SPR sensors are designed for the condition of illumination with large oblique incidence.

The organization of this paper is as follows. In Section 2, the dynamic range of SPR wavelengths for normal mediums that can be obtained by the conventional Kretschmann configuration with a thin metal film is analyzed and the limitation of the conventional Kretschmann SPR configuration in generating IR SPR is described. In Section 3, a specific subwavelength metallic grating structure with high-quality IR SPR is proposed. The IR SPR characteristics and structural parameters for controlling IR SPR are analyzed numerically. In Section 4, the issue of structural optimization is addressed by using a genetic algorithm (GA) to investigate a wide range of structural variations and corresponding SPR behaviors. In Section 5, concluding remarks are given.

2. SPR CHARACTERISTICS OF FLAT METAL FILMS

The most widely used and simplest approach for SPR sensing is the Kretschmann configuration, which employs a prism with a thin metal film, as illustrated in Fig. 1. TM-polarized (*p*-polarized) light illuminated on the thin metal film through the prism effectively excites SP polariton (SPP) at the metal–analyte interface under the SPR condition [1]:

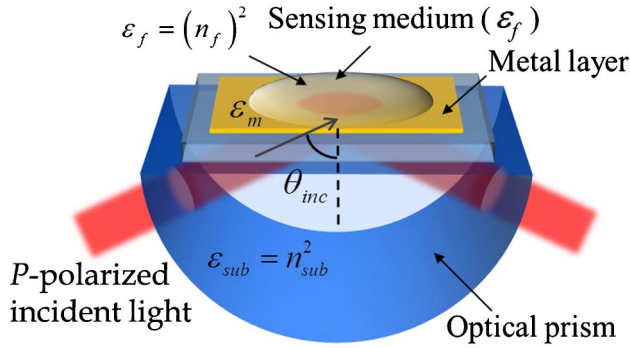


Fig. 1. (Color online) Kretschmann SPR sensor configuration.

$$\frac{2\pi}{\lambda} n_{\text{sub}} \sin \theta_{\text{inc}} = \text{Re}(\beta_{\text{spp}}) \tag{1}$$

with

$$\beta_{\text{spp}} = \frac{2\pi}{\lambda} \sqrt{\frac{\epsilon_m n_f^2}{\epsilon_m + n_f^2}} + \Delta\beta, \tag{2}$$

where n_{sub} is the refractive index of a dielectric substrate (a prism), λ is the wavelength in free space, and θ_{inc} is the incidence angle of the light. The effective SPP propagation constant β_{spp} is determined by factors such as the permittivity of the metal layer ϵ_m and the refractive index of the sensing medium n_f . The term $\Delta\beta$ accounts for the finite thickness of the metal film and the asymmetric configuration due to the prism. At the SPR condition, the incident light is highly absorbed by the metal film and so the SPR wavelength manifests itself at the minimum point in the measured reflection spectrum curve. From Eq. (1), we can see that the SPR wave-

length is determined by the structural parameters, n_{sub} , θ_{inc} , and the thickness of the metal layer [1,10].

It was of interest to investigate the possible values of SPR wavelengths and find fundamental limitation in the dynamic range of SPR wavelengths of the Kretschmann configuration. The SPR wavelengths (defined as the wavelengths producing the maximum loss in the reflection spectrum curve) were analyzed with wide variations in the substrate refractive index n_{sub} and the light incidence angle θ_{inc} in aqueous solution ($n_f = 1.33$). The results of the analysis of the SPR wavelength range for thin metal films with a thickness of 40, 50, and 60 nm are presented in Figs. 2(a)–2(c). From these results, we can see, first, that with small values of n_{sub} and θ_{inc} , SPR can be induced with wavelengths very far in the IR region. The regions colored with oxblood red (upper left corner in Fig. 2) indicate the configurations of n_{sub} and θ_{inc} , where the SPR wavelengths were evaluated to be more than 2400 nm. Second, for large incidence angles, it was more difficult to realize IR SPR with normal dielectric materials because the refractive index of the dielectric substrate for IR SPR tends to move toward a lower value. This is an interesting point because, in typical cases of fiber optic SPR sensors, the light rays of the guided optical mode are incident on the thin metal coating layer, which is deposited around the bare fiber core with its cladding removed, with a large incidence angle. For example, with a fixed incidence angle of 85° and the normal material configurations of Au film and SiO_2 substrate, the calculated SPR wavelengths for continuously varying thicknesses of Au film were located in the visible wavelength region below the 700 nm wavelength, as plotted in Fig. 2(d). This lack of a fundamental mechanism for inducing IR SPR hinders the formation of a high-quality fiber optic IR SPR sensor using the normal Kretschmann SPR configuration.

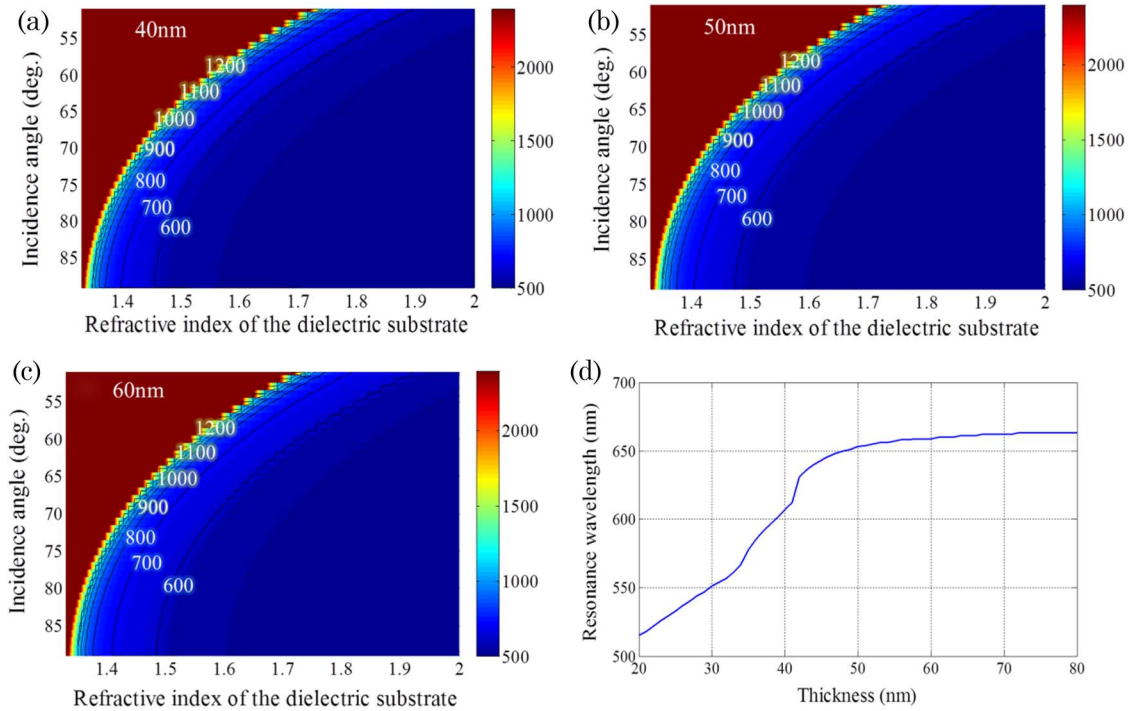


Fig. 2. (Color online) SPR wavelengths in the Kretschmann configuration calculated with variations in the substrate refractive index and incidence angle of illumination for Au films with thicknesses of (a) 40, (b) 50, and (c) 60 nm. The outer medium is water ($n_f = 1.33$). (d) Calculated SPR wavelengths for SiO_2 substrate and Au films with continuously varying thicknesses and an incidence angle of 85° .

3. IR SPR CHARACTERISTICS OF THE SUBWAVELENGTH METALLIC GRATING

In this section, a subwavelength metallic grating that can induce IR SPR with a narrow and deep resonance spectrum appropriate for high-performance IR SPR sensing applications is proposed. We consider that the surface corrugation of a metal film taking the form of a subwavelength metallic grating can modify the SPR characteristics even under illumination with a large incidence angle of about 85°. A method of structuring metallic surfaces in the subwavelength scale in order to change the SP dispersion has been devised for the terahertz region [11,12]. The effective bound surface mode on the subwavelength-scale structured interface is referred to as “spoof SP.” We extend the concept of spoof SP to the near-IR wavelength region. Based on the observation that there is a region in which IR SPR does not exist, we designed a kind of spoof IR SP structure to modify the SP dispersion relation and induce spoof IR SPR in the region where IR SPR is nonexistent. More specifically, this paper shows that the subwavelength metallic grating structure could shift the SPR wavelength toward the IR band through the spoof SP effect. In the near-IR wavelength region, a metallic layer cannot be treated as a perfect conductor, therefore, the effective refractive index of the spoof SP mode depends heavily on the permittivity value of the metal as well as its geometric structures [13–15]. In this paper, the SP modes and the IR SPR characteristics are analyzed with rigorous coupled-wave analysis (RCWA) [16].

The proposed IR SPR subwavelength grating structure is illustrated in Fig. 3(a). The proposed structure consists of

three layers: a subwavelength metallic (Au) binary grating, a thin bottom metal (Au) layer, and a fused silica substrate with a permittivity value of ϵ_{SiO_2} in an aqueous environment similar to the conventional Kretschmann SPR configuration. The combination of Au and fused silica is appropriate for SPR sensing of low-refractive-index materials in an aqueous environment. The grating depth of the subwavelength grating, the permittivity value of Au, the period, the fill factor, and the thickness of the thin bottom metal layer are denoted by h_1 , ϵ_{Au} , w_1 , $f = (w_1 - w_2)/w_1$, and h_2 , respectively [Fig. 3(a)].

TM-polarized plane waves with a fixed incidence angle of θ_{inc} but different wavelengths were incident and reflected on the thin bottom metal layer of the grating through the transparent fused silica layer. The spectral interrogation was numerically analyzed with varying of the environmental refractive index [Fig. 3(b)]. When the environmental refractive index was varied in the range 1.30–1.37, the SPR wavelength moved continuously in the range 900–1200 nm. An example grating structure tuned to a resonance wavelength of 1000 nm with its structural parameters set to $w_1 = 170$ nm, $w_2 = 55$ nm, $h_1 = 40$ nm, and $h_2 = 28$ nm was analyzed. In RCWA, the permittivity values of the dielectric substrate ϵ_{SiO_2} and the Au layer ϵ_{Au} are modeled by the frequency-dependent material data on the SOPRA database [17]. The incidence angle θ_{inc} of the excitation plane waves was set to 85°. Such a large incidence angle was used with the expectation of application to fiber optic IR SPR sensors.

The sensitivity is defined and used as the evaluation factor for the quality of SPR. When, at the SPR condition, the refractive index of the sensing medium is altered by δn_f , the SPR wavelength shifts by $\delta \lambda_{\text{res}}$. Then, the sensitivity is defined as [1]

$$S = \frac{\delta \lambda_{\text{res}}}{\delta n_{\text{eff}}} \frac{\delta n_{\text{eff}}}{\delta n_f}, \quad (3)$$

where n_{eff} and $\delta n_{\text{eff}}/\delta n_f$ are given by $n_{\text{eff}} = \text{Re}(\beta_{\text{SP}}/k_0)$ and $\frac{\delta n_{\text{eff}}}{\delta n_f} \approx \text{Re}\left(\frac{\epsilon_{\text{Au}}}{\epsilon_{\text{Au}} + n_f^2}\right)^{3/2}$. Here, k_0 is the free space wavenumber. The unit for S is nanometer per refractive index unit (RIU). In the analysis shown in Fig. 3(b), the average sensitivity of 3900 nm/RIU was obtained in the interval of the refractive index change Δn_f from 1.33 to 1.34. This is similar to the usual sensitivity of conventional SPR on a flat metal layer in the visible band [5,18]; this example thus confirms that the IR SPR has a level of sensitivity similar to that of the visible SPR.

For this example grating structure, the effects of structural parameters w_1 , w_2 , h_1 , and h_2 on the SPR structure were analyzed. From the simulation analysis of several grating structures with different specifications, we observed that the binary grating layer parameterized by w_1 , w_2 , and h_1 specifies the position of the SPR wavelength and that the bottom metal layer with finite thickness h_2 has a critical role in refining the SPR profile at the SPR wavelength determined by the binary grating layer.

The effective permittivity [11–15] and effective SP modes of the binary grating layer can be understood through a dispersion-relation analysis of the effective SP modes (see Appendix A) [19,20]. As the thickness of the subwavelength grating increases, the relative portion of the electromagnetic field confined within the subwavelength grating also increases because of the deep penetration of the electromagnetic field

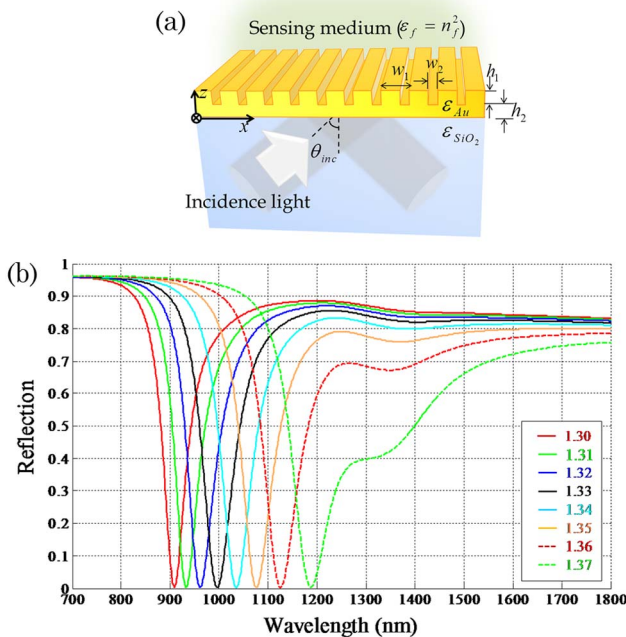


Fig. 3. (Color online) (a) SPR sensor structure with the proposed grating structure with permittivity of ϵ_{SiO_2} for the substrate and ϵ_{Au} for the deposited Au metal layer. The surface metallic grating has a period of w_1 , width of engraved part w_2 , grating depth h_1 , and thickness of bottom metal layer h_2 . (b) Reflection spectra of the grating structure with changes in the environment refractive index from 1.30 to 1.37 (left to right) with $w_1 = 170$ nm, $w_2 = 55$ nm, $h_1 = 40$ nm, and $h_2 = 28$ nm (analyzed by RCWA).

into the grating region through the dielectric part of the grating. The effective index of the SP mode is heavily dependent on the relative portion of the electromagnetic fields between the metallic and dielectric mediums. Thus, it is intuitive that the propagation constant (effective refractive index) of the SP modes increases with the grating thickness because of the increase in the relative ratio of the electromagnetic field confined in the metallic layer.

To clarify the role of h_1 among the three parameters of w_1 , w_2 , and h_1 , the reflection spectra were analyzed with varying h_1 for the example grating structure tuned to 1000 nm SPR. The reflection spectra analyzed with h_1 varying from 20 to 80 nm and fixed values of $w_1 = 170$ nm and $w_2 = 55$ nm are plotted in Fig. 4(a); the position of SPR was controllable in the range from 750 to 1700 nm for this h_1 range. The obtained spectra show that the depth and narrowness of the SPR are degraded as the SPR moved to the longer wavelength region. Although the parameters w_1 , w_2 , and h_1 contribute mainly to determining the position of the SPR wavelength, they have to be optimized simultaneously to obtain the optimal SPR sensitivity and spectrum narrowness. The topic of optimization is addressed in Section 4.

Figure 4(b) presents the critical role of the bottom layer thickness, h_2 . As shown in the spectrum for $h_2 = 0$ nm, the subwavelength grating structure could not sustain the well-defined single resonance feature without the aid of the bottom metal layer. Several randomized dips appear in the spectrum in this case. However, with increasing thickness, the bottom metallic layer started to refine the SPR feature progressively

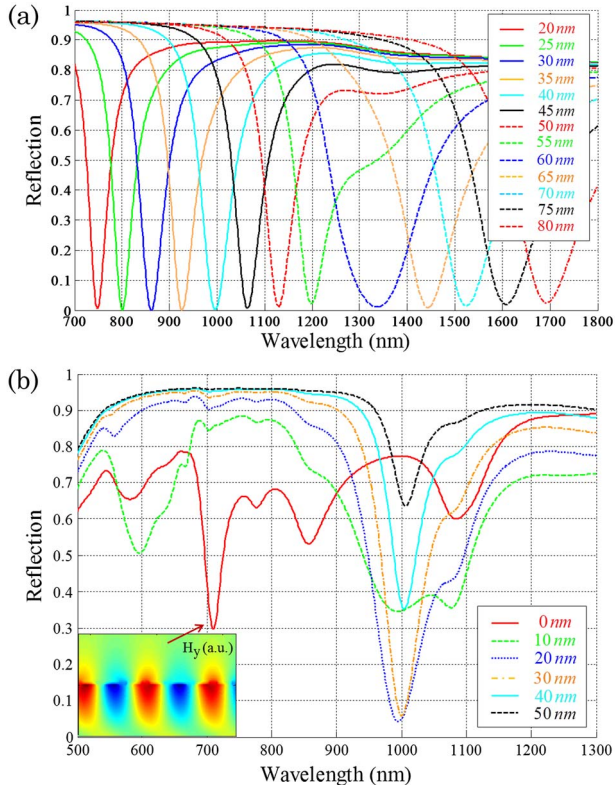


Fig. 4. (Color online) Reflection spectra of the sampled metallic grating with variation of the (a) grating depth h_1 and the (b) thickness of the bottom thin metal layer h_2 . Inset: H_y field distribution obtained for $h_2 = 0$ nm at $\lambda = 700$ nm.

without the SPR wavelength position being changed (in this case, at 1000 nm). A comparison of the results for $h_2 = 30$ nm and $h_2 = 50$ nm confirms that there is an optimal value of h_2 for specifying the best quality of SPR for the fixed parameters w_1 , w_2 , and h_1 . The bottom flat metal layer is expected to prevent unwanted resonance modes (see the inset in Fig. 4(b)] at the interface between the substrate and the binary metallic grating layer, and then enhances the coupling efficiency of incident light with a single SP mode [21–23].

As seen, the grating structure parameters w_1 , w_2 , and h_1 and the bottom metal layer thickness h_2 had different roles in shaping the SPR behavior. However, to achieve optimal IR SPR, all four parameters need to be considered.

4. OPTIMIZATION OF IR SPR SUBWAVELENGTH METALLIC GRATINGS

To optimize the proposed IR SPR structure, a four-dimensional search that considers all four parameters simultaneously is required. In this paper, the GA combined with RCWA was employed as an optimization tool. The GA is a nonlinear evolutionary search technique used in a wide range of nonlinear optimization problems [24]. The GA tries to change the structural parameters, but RCWA gives the reflection spectra of the structure specified by the GA. RCWA was used to obtain the value of the objective function (merit function) within the GA framework.

The objective function of the GA is designed as [25,26]

$$F(P_k) = \sqrt{\sum_{j=1}^4 \left(a_j \left(\frac{y_j - y_{j,\text{ref}}}{y_{j,\text{ref}}} \right) \right)^2}, \quad (4)$$

where k is the iteration number, P_k is the population with population size m , and y_1, y_2, y_3 , and y_4 are the measures of the bandwidth of the SPR resonance curve, the SPR wavelength, the SPR dip depth, and the sensitivity, respectively. $y_{j,\text{ref}}$ is the target value of the respective parameter (y_j) and a_j is the weighting ratio of each evaluation factor, which is normalized as $\sum_{j=1}^4 a_j^2 = 1$. The unknown variables to be optimized were the period w_1 , the engraved portion w_2 , the grating depth h_1 , and the thickness of the bottom metal layer h_2 . The incidence angle of the external plane wave was set to 85° . The GA optimization was performed for the three wavelengths of 1100, 1300, and 1500 nm. For the optimization, the weight of the SPR wavelength a_2 was set to $\sqrt{0.5}$, and the other weight numbers

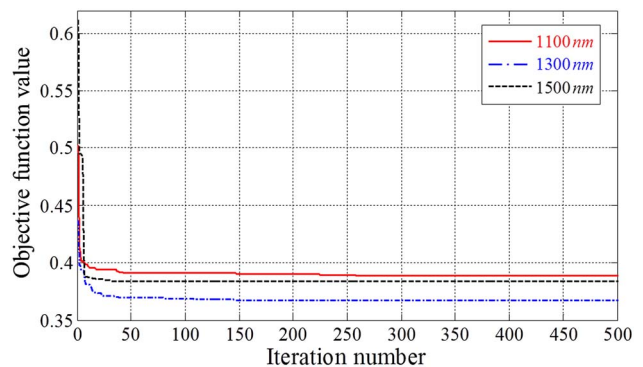


Fig. 5. (Color online) Convergence of the objective function with iteration for three target wavelengths.

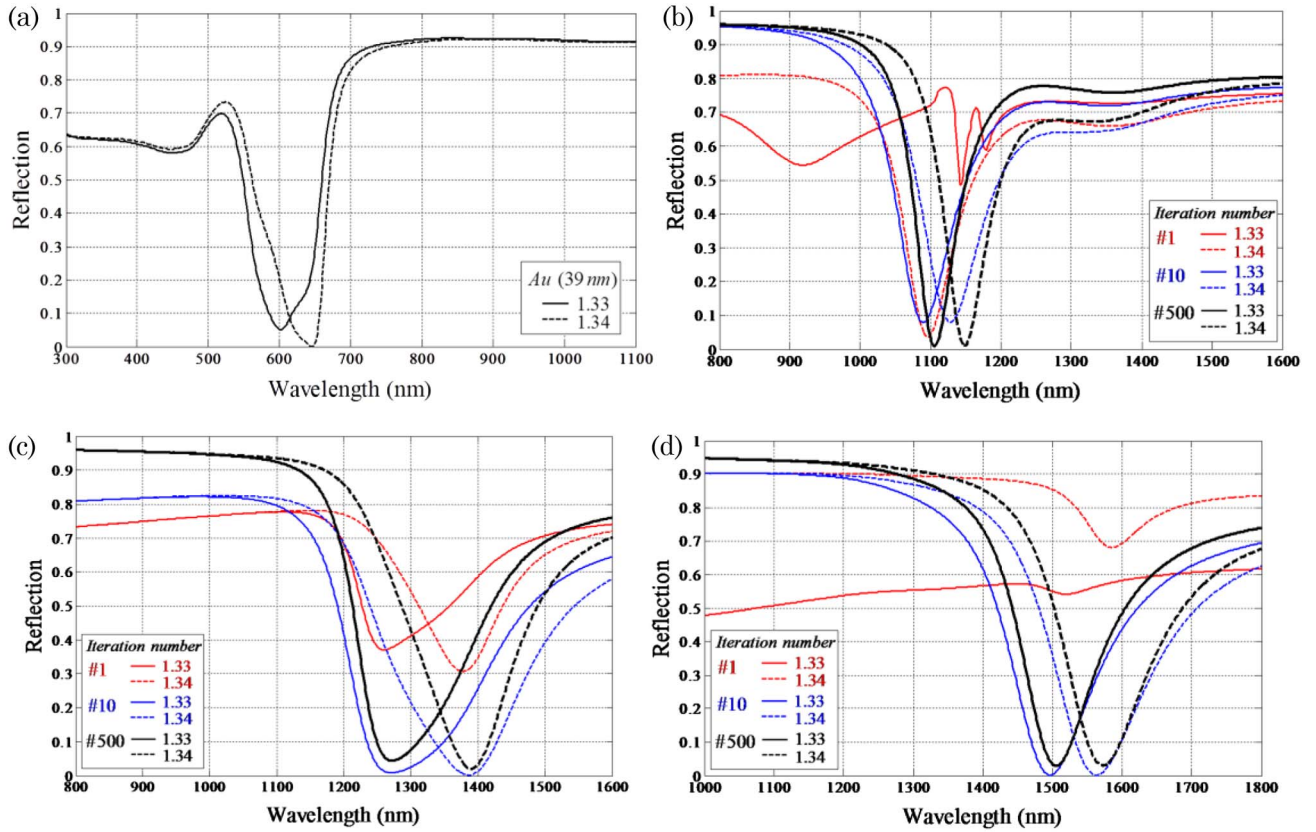


Fig. 6. (Color online) Numerically optimized results of the (a) flat Au layer and Au grating layer for the target wavelength set to (b) 1100, (c) 1300, and (d) 1500 nm. The reflection spectra of the metallic grating on the surface of the Au layer as the GA progresses are presented. The refractive indices of the outer material are 1.33 and 1.34.

a_1 , a_3 , and a_4 were all set to $\sqrt{0.5/3}$. The sensitivity was evaluated within the variation of the refractive index from 1.33 to 1.34. Figure 5 shows the convergence of the objective function of the GA for the three target wavelengths.

The corresponding plots for the evolution of the reflection spectra for the three target SPR wavelengths are presented in Figs. 6(b)–6(d). The best spectra obtained at each of the initial, tenth, and 100th iteration stages in the GA are presented together in each figure. In addition, for comparison, the spectra measured for the environmental refractive indices of 1.33 and 1.34 are plotted, denoted by colored solid and dashed curves, respectively. For the target SPR wavelength of 1100 nm, a reflection spectrum with 76 nm bandwidth and 4300 nm/RIU sensitivity was obtained. For 1300 nm, a spectrum with 207 nm bandwidth and 11800 nm/RIU sensitivity was obtained, and, for 1500 nm, a spectrum with 150 nm bandwidth and 6800 nm/RIU sensitivity was obtained. It has been

shown that the proposed subwavelength metallic grating structure appropriately managed high-quality IR SPR for IR sensing applications. For comparison, presented in Fig. 6(a) is the reflection SPR spectrum of the optimized Kretschmann flat metal structure tuned to the wavelength of 602 nm, with a sensitivity of 4400 nm/RIU in aqueous medium and a bandwidth of 110 nm. The results of the GA optimization are summarized in Table 1. As discussed previously, the bottom metal layer with finite thickness was critical for achieving a high-quality SPR spectrum. The optimization results reflect this property of the bottom metal layer. In Table 1, the figure of merit (FOM) [27] defined by

$$FOM = \frac{S}{BW} \quad (5)$$

is shown as an additional evaluation factor, where BW and S denote the FWHM (bandwidth) of an SPR dip and the

Table 1. Comparison of Flat Au and Optimization Results of Subwavelength Metallic Grating for IR Sensing at Different Wavelengths

Structural Parameters $w_1/w_2/h_1/h_2$ (nm)	Resonance Wavelength (nm)	Sensitivity (nm/RIU)	Bandwidth (nm)	FOM (RIU ⁻¹)	Sensing Range (RIU)
Flat Au (39)	602	4400	110	40.0	1.33–1.34
176/70/47/30	1105	4300	76	56.6	1.33–1.34
203/67/61/29	1272	11800	207	57.0	1.33–1.34
239/80/75/28	1505	6800	157	43.3	1.33–1.34

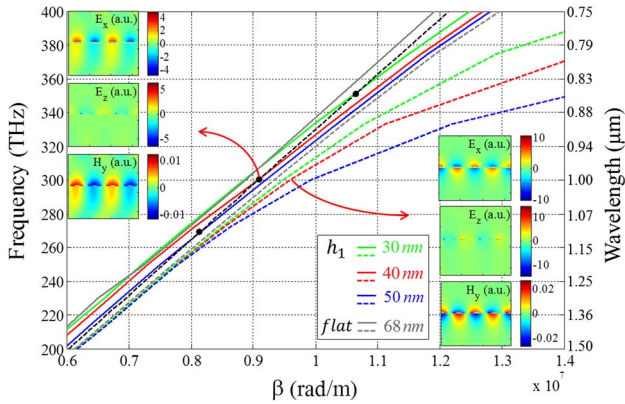


Fig. 7. (Color online) Dispersion characteristics of the surface grating layer for different grating depths (30, 40, and 50 nm). In all cases, the grating period and engraved portion were fixed at 170 and 55 nm, respectively. Each grating depth has two SP modes: symmetric (left insets) and asymmetric (right insets) modes. The dispersion characteristics for the incident light from the substrate are represented as black dashed curves: intersections of the latter with other dispersion lines indicate where SPR can occur. The inserted field distributions are for surface modes with 40 nm depth at a 1000 nm wavelength, marked by red arrows.

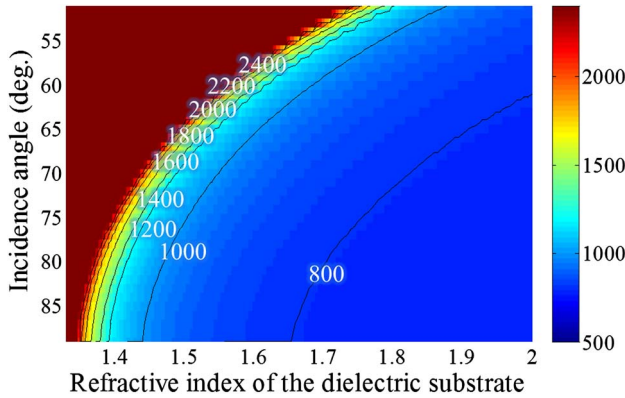


Fig. 8. (Color online) SPR wavelengths in the proposed grating structure ($w_1 = 170$ nm, $w_2 = 55$ nm, $h_1 = 40$ nm, $h_2 = 28$ nm) calculated with variations in the substrate refractive index and incidence angle of illumination.

sensitivity, respectively. The unit of FOM is RIU^{-1} . SPR that exhibits a higher FOM has higher resolution in most SPR sensing applications. A comparison of the FOM value of the optimized IR SPR with that of the visible SPR shows an improvement in the FOM of three IR SPRs over the conventional SPR (Table 1). We have thus numerically demonstrated the generation of IR SPR using the proposed subwavelength metallic grating structure and have provided an effective optimal method of the subwavelength metallic grating for specific IR SPRs.

5. CONCLUSION

In conclusion, it was shown that the proposed subwavelength metallic grating structure provided high-quality IR SPR under the condition of large incidence angle illumination. The numerical study using the optimal design method with a combination of GA and RCWA shows that a wide range of SPR wavelengths was possible and that functional factors such as sensitivity, resonance curve bandwidth, and FOM, as well

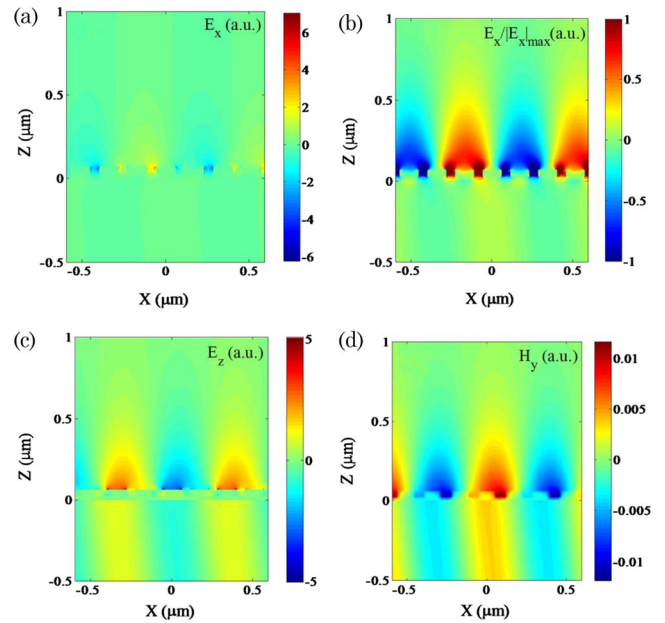


Fig. 9. (Color online) Field distributions of (a) E_x , (b) normalized field distribution of $E_x/E_{x\text{max}}$, (c) E_z , and (d) H_y in the grating structure at SPR at the 1000 nm free space wavelength.

as SPR wavelength, could be enhanced compared with those obtained using the conventional Kretschmann configuration in the visible range. One of the main findings is that the bottom metal layer with finite thickness is a key structural factor of the proposed subwavelength grating structure for enhancing the functional features of IR SPR. The IR SPR excitation and its generation method demonstrated in this paper can be used as fundamental elements for IR SP nanophotonics as well as IR SPR sensing applications.

APPENDIX: SPR DISPERSION RELATION ON METALLIC GRATINGS

Dispersion relations of the SP modes on the proposed grating structure are numerically derived using the local Fourier modal method [28]. The effects of grating depths h_1 of 30, 40, and 50 nm on the dispersion relation are plotted in Fig. 7. As observed, there are two SP modes at each grating depth—phase-symmetric (solid curves) and phase-asymmetric modes (dashed curves)—but only the symmetric modes meet the light line of the incident light in the SiO_2 substrate layer (indicated by the black dashed curve). The crossing points are marked by black dots (Fig. 7). The insets show the field distributions of SP modes at a wavelength of 1000 nm (indicated by arrows). By slightly varying the grating depth (± 20 nm), we can observe the change in dispersion characteristics that the matched (excitation) wavelength between the incident light and the symmetric SP modes moves in the range of about 860–1130 nm. To confirm the surface grating effect, a dispersion line of the SP modes on a flat metal with $h_1 = 0$ nm and $h_2 = 68$ nm is inserted for comparison with corrugated metal with $h_1 = 40$ nm and $h_2 = 28$ nm for 1000 nm resonance. The SPR wavelengths of the proposed grating structure ($w_1 = 170$ nm, $w_2 = 55$ nm, $h_1 = 40$ nm, $h_2 = 28$ nm) in aqueous solution ($n_f = 1.33$) are analyzed with wide variations in the substrate refractive index n_{sub} and light incidence angle θ_{inc} (Fig. 8).

The detailed field distributions of the SP mode excited at a wavelength of 1000 nm under the SPR condition are presented in Fig. 9. The electric field (E_x) in the x direction is greatly enhanced inside the grating groove and the z -directional electric field (E_z) is dominantly excited at the flat metal portions.

ACKNOWLEDGMENTS

This work was supported by the National Research Foundation and the Ministry of Education, Science and Technology of Korea through the Creative Research Initiatives Program (Active Plasmonics Application Systems).

REFERENCES

1. J. Homola and O. S. Wolfbeis, *Surface Plasmon Resonance Based Sensors* (Springer, 2006), Vol. 4.
2. O. S. Wolfbeis, "Fiber-optic chemical sensors and biosensors," *Anal. Chem.* **80**, 4269–4283 (2008).
3. B. Lee, S. Kim, H. Kim, and Y. Lim, "The use of plasmonics in light beaming and focusing," *Prog. Quantum Electron.* **34**, 47–87 (2010).
4. B. D. Gupta and R. K. Verma, "Surface plasmon resonance-based fiber optic sensors: principle, probe designs, and some applications," *J. Sensors* **2009**, 979761 (2009).
5. B. Lee, S. Roh, and J. Park, "Current status of micro- and nano-structured optical fiber sensors," *Opt. Fiber Technol.* **15**, 209–221 (2009).
6. W. Ding, S. R. Andrews, T. A. Birks, and S. A. Maier, "Modal coupling in fiber tapers decorated with metallic surface gratings," *Opt. Lett.* **31**, 2556–2558 (2006).
7. R. K. Verma and B. D. Gupta, "Surface plasmon resonance based fiber optic sensor for the IR region using a conducting metal oxide film," *J. Opt. Soc. Am. A* **27**, 846–851 (2010).
8. J. Homola, I. Koudela, and S. S. Yee, "Surface plasmon resonance sensors based on diffraction gratings and prism couplers: sensitivity comparison," *Sens. Actuators B Chem.* **54**, 16–24 (1999).
9. R. Kashyap and G. Nemova, "Surface plasmon resonance-based fiber and planar waveguide sensors," *J. Sensors* **2009**, 645162 (2009).
10. S. Patskovsky, A. V. Kabashin, M. Meunier, and J. H. T. Luong, "Properties and sensing characteristics of surface plasmon resonance in infrared light," *J. Opt. Soc. Am. A* **20**, 1644–1650 (2003).
11. J. B. Pendry, L. Martín-Moreno, and F. J. García-Vidal, "Mimicking surface plasmons with structured surfaces," *Science* **305**, 847–848 (2004).
12. N. Yu, Q. J. Wang, M. A. Kats, J. A. Fan, S. P. Khanna, L. Li, A. G. Davies, E. H. Linfield, and F. Capasso, "Designer spoof surface plasmon structures collimate terahertz laser beams," *Nat. Mater.* **9**, 730–735 (2010).
13. C. H. Gan and P. Lalanne, "Well-confined surface plasmon polaritons for sensing applications in the near-infrared," *Opt. Lett.* **35**, 610–612 (2010).
14. E. Popov, S. Enoch, and N. Bonod, "Absorption of light by extremely shallow metallic gratings: metamaterial behavior," *Opt. Express* **17**, 6770–6781 (2009).
15. A. V. Kabashin, P. Evans, S. Pastkovsky, W. Hendren, G. A. Wurtz, R. Atkinson, R. Pollard, A. V. Podolskiy, and A. V. Zayats, "Plasmonic nanorod metamaterials for biosensing," *Nat. Mater.* **8**, 867–871 (2009).
16. H. Kim, I.-M. Lee, and B. Lee, "Extended scattering-matrix method for efficient full parallel implementation of rigorous coupled-wave analysis," *J. Opt. Soc. Am. A* **24**, 2313–2327 (2007).
17. SOPRALAB, N&K database, <http://www.sopra-sa.com/index2.php?goto=dl&rub=4>.
18. B. Lee, S. Roh, H. Kim, and J. Jung, "Waveguide-based surface plasmon resonance sensor design," *Proc. SPIE* **7420**, 74200C (2009).
19. S. G. Rodrigo, L. Martín-Moreno, A. Y. Nikitin, A. V. Kats, I. S. Spevak, and F. J. García-Vidal, "Extraordinary optical transmission through hole arrays in optically thin metal films," *Opt. Lett.* **34**, 4–6 (2009).
20. Q. Gan, Z. Fu, Y. J. Ding, and F. J. Bartoli, "Bidirectional sub-wavelength slit splitter for THz surface plasmons," *Opt. Express* **15**, 18050–18055 (2007).
21. S. A. Darmanyan and A. V. Zayats, "Light tunneling via resonant surface plasmon polaritons states and the enhanced transmission of periodically nanostructured metal films: an analytical study," *Phys. Rev. B* **67**, 035424 (2003).
22. F. J. García-Vidal, L. Martín-Moreno, T. W. Ebbesen, and L. Kuipers, "Light passing through subwavelength apertures," *Rev. Mod. Phys.* **82**, 729–787 (2010).
23. R. Gordon, A. G. Brolo, D. Sinton, and K. L. Kavanagh, "Resonant optical transmission through hole-arrays in metal films: physics and applications," *Laser Photon. Rev.* **4**, 311–335 (2010).
24. Z. Michalewicz, *Genetic Algorithms + Data Structures = Evolution Programs* (Springer, 1999).
25. S. Roh, T. Chung, and B. Lee, "Overview of the characteristics of micro- and nano-structured surface plasmon resonance sensors," *Sensors* **11**, 1565–1588 (2011).
26. D. Choi, Y. Lim, S. Roh, I.-M. Lee, J. Jung, and B. Lee, "Optical beam focusing with a metal slit array arranged along a semicircular surface and its optimization by genetic algorithm," *Appl. Opt.* **49**, A30–A35 (2010).
27. B. Špačková, M. Piliarik, P. Kvasnička, C. Themistos, M. Rajarajan, and J. Homola, "Novel concept of multi-channel fiber optic surface plasmon resonance sensor," *Sens. Actuators B Chem.* **139**, 199–203 (2009).
28. H. Kim and B. Lee, "Mathematical modeling of crossed nanophotonic structures with generalized scattering-matrix method and local Fourier modal analysis," *J. Opt. Soc. Am. B* **25**, 518–544 (2008).